Three-dimensional detection of a gas-liquid interface by means of oblique colored light sources

Maximilian Dreisbach[1,*], Sebastian Blessing[1], Frank Michaux[2], André Brunn[2], Alexander Stroh[1], Jochen Kriegseis[1]

[1] Institute of Fluids Mechanics, Karlsruhe Institute of Technology, Germany
[2] ILA_5150, Kurbrunnenstraße 24, 52066 Aachen, Germany
*Corresponding author: maximilian.dreisbach@kit.edu

Keywords: Shadowgraphy, Drop Impact, RGB-Imaging, Colored Light Sources, Color Correction, Gas-Liquid Interface

ABSTRACT

The present work introduces an extension of the shadowgraphy method by differently colored oblique light sources for the observation of the three-dimensional dynamics during drop impingement. The wetting of a flat or structured surface by an impinging droplet is relevant for many technical processes and therefore a further understanding of the drop impact dynamics is essential for an optimization of these processes. The most widely used optical measurement technique for drop impact experiments is the shadowgraphy method, which produces a clear two-dimensional representation of the gas-liquid interface. However, drop impact dynamics – especially on structured surfaces – are inherently three-dimensional. Therefore, two lateral light sources are introduced, in order to produce glare points on the gas-liquid interface that reveal additional three-dimensional information of the droplet shape. Narrow-banded LEDs with distinct spectra and maxima in the visible light illuminate the droplet from different angles in red, green and blue light, respectively, while a high-speed RGB-camera captures the images produced by each light source in the corresponding image channel, therefore creating three unique views of the droplet. Thereby the shadowgraphy image resulting from the blue backlight illumination is recorded in the blue image channel, while the glare points from the green and red lateral light sources are captured in the accordingly remaining channels. In order to compensate for the mutual perturbation of the images resulting from cross-talk between the channels and the polychromatic light of the LEDs, a color correction is introduced, which is based on the transfer function between the light sources and the channels of the RGB-camera. The transfer function is determined by a spectral integration over the power distribution of the individual light sources and sensitivities of the single camera channels likewise, with the assumptions of fully specular reflection and that the spectral distribution of the reflected light equals the incoming light. In experiments with the proposed measurement setup of a water droplet impinging on a flat substrate it is successfully demonstrated, that three unique and independent grayscale images can be reconstructed with this color correction function, which successfully removes the mutual perturbations. The presented method is a pure addition to the shadowgraphy method, as it produces a clear shadowgraphy image and optionally provides two further unique views by glare points on the gas-liquid interface within a single RGB-camera setup.

1. Introduction

The impact of liquid droplets on both wet and dry surfaces is a key process for a wide range of technical applications. For example, in spray cooling an optimization of the interaction between the droplet and the solid wall can lead to significant gains in efficiency (Ashgriz, 2011) and for spray coating a prevention of an air inclusion would improve the quality of the surface. Various details of these processes, however, remain yet to be fully understood (Josserand & Thoroddsen, 2016). Drop impact phenomena include splashing, receding, partial or complete rebound and deposition of the impinging droplet and depend on the impact conditions – most importantly the velocity and size of the droplet, the angle of incidence, as well as the fluid properties and the roughness of the substrate (Yarin, 2005). A commonly used optical measurement method for the observation of drop impact dynamics is the shadowgraphy technique (Wakeham et al., 2007; Nitsche & Brunn, 2006), wherein the falling droplet is illuminated in parallel backlight, mapping the contour of the droplet accurately and therefore allowing for a precise measurement of the gas-liquid interface. In combination with high speed imaging this method can be used to measure the wetting properties and contact line dynamics of drops impacting at different relative velocities on smooth, rough or structured surfaces (Rioboo et al., 2001).

(a) frame before impact (b) frame of impact (c) first frame after impact (d) third frame after impact

Figure 1. Shadowgraphy images of a water droplet impinging on a substrate with SiOx-coating, produced in a standard shadowgraphy setup with a blue backlight LED; (a,b) gray-scale conversion of the blue color channel to mimic monochromatic imaging, (c,d) full RGB-image, revealing the direct transmission of the blue background illumination.

The present work addresses the deposition type drop impact, as characterized by Rioboo et al. (2002). Resulting shadowgraphy images for a water droplet impacting on a smooth hydrophobic surface can be seen in Figure 1. However, these measurements provide only a two-dimensional representation of the drop shape, whereas the drop dynamics is inherently three-dimensional, especially in the non-equilibrium phase of the impact. While numerical simulations can deliver a three-dimensional representation of the droplet (Fink et al., 2018; Wörner et al., 2021), their model functions for the contact angle dynamics rely on measured droplet characteristics from experiments (Kistler, 1993; Cox, 1986). Furthermore these simulations have to be validated on adequate experimental data. The validation is rendered difficult due to the lack of an accurate three-dimensional representation of the gas-liquid interface in experimental data. Therefore, in the present study an optical measurement method based on the shadowgraphy technique is investigated which captures additional three-dimensional information of the droplet during impact

by using light sources with different colors to produce reflective images from different azimuthal angles on the droplet surface in a single RGB-image.

2. Experimental Setup

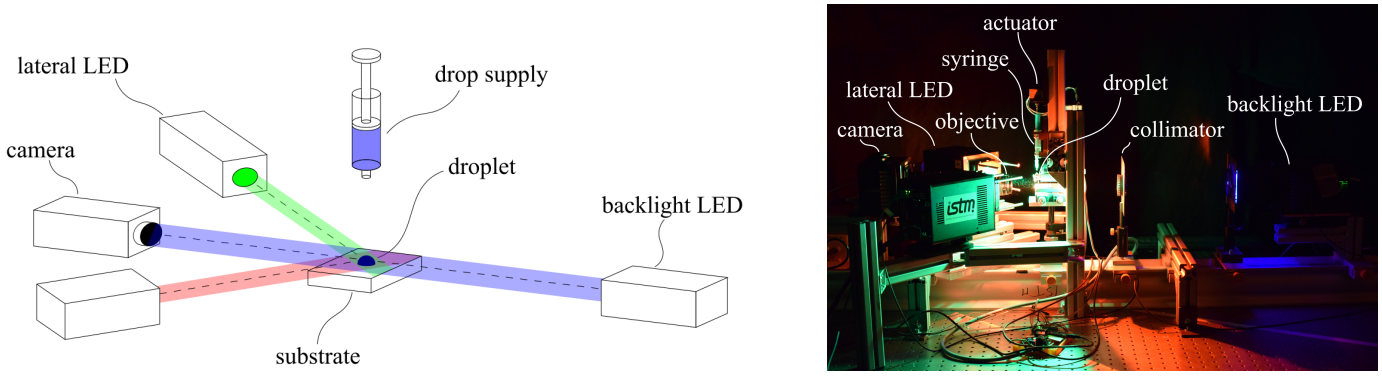

(a) sketch (b) photograph

Figure 2. Sketch (a) and photograph (b) of the experimental setup of the applied RGB-shadowgraphy method.

The present approach extends the shadowgraphy method by supplementing two lateral light sources to the standard shadowgraphy setup as shown in Figure 2. These additional light sources are positioned in one horizontal plane and symmetrically at an angle to the optical axis which aligns the camera with the droplet and backlight. In order to ensure a reproducible droplet volume over multiple experiments and to avoid oscillations of the droplet from the introduction of momentum the droplet is produced by an automatic drop application system consisting of a syringe with a cannula diameter of $d_s = 0.1$mm and a stepper motor with $l = 10$mm linear displacement and a step angle of $\alpha = 7.5°$, which is used as a linear actuator for the syringe. Choosing water at room temperature as the droplet medium results in a $D \approx 2$mm diameter droplet. The substrate has a hydrophobic surface created by a silicon oxide (SiOx) coating. The two lateral light sources, as well as the backlight are high-power *ILA_5150 LPSv3* LEDs with narrow-banded spectra and maxima in the visible spectrum at $\sim$ 455nm ("*blue*"), $\sim$ 521nm ("*green*"), $\sim$ 632nm ("*red*") for the desired blue, green and red light sources, respectively. The light of the LEDs is captured at 3.000 frames per second (fps) by a *Photron Fastcam Mini WX* RGB-Camera, equipped with a *Schneider-Kreuznach Apo-Componon* 4.0/60 enlarging lens, where the three-colors $i =$ ("*red*", "*green*", "*blue*") of illumination are expected to be mainly captured with the corresponding channels of the RGB camera chip.

The backlight produces a classical shadowgraphy image on the corresponding image channel, where only light which is not deflected on the interface of the droplet reaches the camera chip. In order to capture the shape of the droplet as accurately as possible a parallel light beam is required. This is achieved by placing an optical collimator consisting of a pinhole aperture with a diameter of $d_a = 4$mm and a *Spindler & Hoyer* biconvex collimator lens with 300mm focal length between the backlight and the droplet. For the backlight a blue LED is used since the chip of the camera

possesses the lowest relative sensitivity in this range of wavelengths and the highest response in the chip of the camera is expected from the backlight LED, since the light path reaches the camera directly, thus requiring a lower intensity than the other channels. The lateral light sources are focused by plano-convex lenses with a broadband anti-reflective coating (reflectivity $< 0.5\%$) from *Thorlabs* and illuminate the droplet from an azimuthal angle lower than $90°$ in respect to the camera, therefore only reflected light reaches the camera. Since the light is partially transmitted at the first interface between air and water, it is reflected again on the following interfaces in the path of the light ray, for example while leaving the droplet (van de Hulst & Wang, 1991) or at internal phase boundaries of air inclusion within the droplet. Due to the smooth surface of the phase boundary, the reflection is consider to be pure interface reflection, which is captured by the camera as differently coloured glare points on each side of the droplet and on any present air bubbles, thereby encoding additional volumetric information on the droplet in the remaining red and green image channels. Since the information is separated between the channels of the RGB-image, three individual grayscale images with accordingly different illumination conditions can be extracted from the RGB-image, each providing a unique representation of the droplet that can be used for the volumetric reconstruction of the droplet.

3. Image Processing

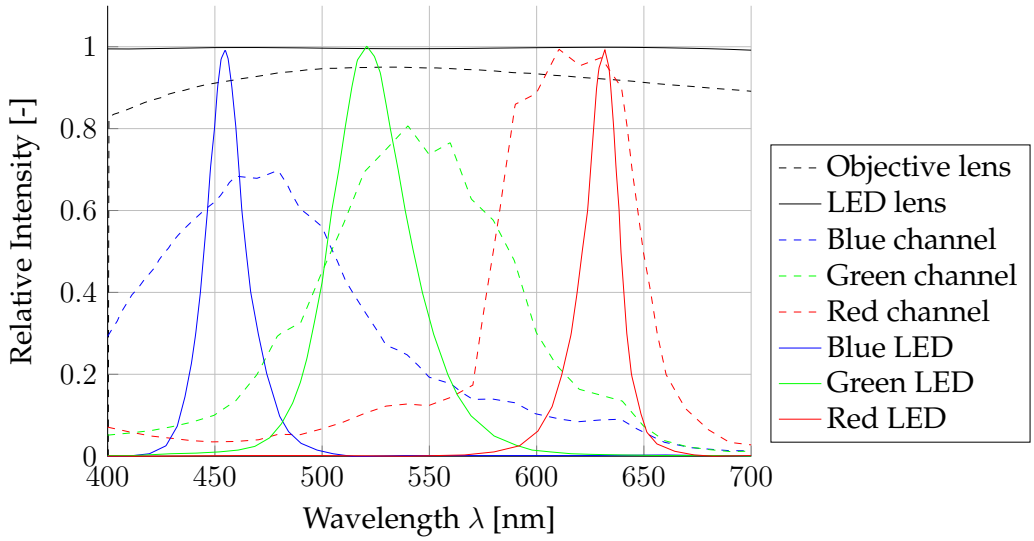

Figure 3. Spectral power distribution of the LED light sources (color-coded solid lines), spectral sensitivity distribution of the camera's color channels k (color-coded dashed lines), transmittance of the objective lens (dashed black line) and the collimator lenses of the light sources (solid black line).

As can be seen in Figure 3 the spectral power distribution of the light sources do not perfectly match with the spectral sensitivity of the corresponding camera channels k =(R, G, B). Therefore, each light source causes a perturbation of the images in the other channels, which consequently needs to be considered as follows.

The response of the k^{th} color channel at pixel p on the camera chip $I_k(p)$ can be calculated by spectral integration from the spectral power distribution (SPD) of the incoming light $L(\lambda)$, the spectral transmittance of the color filter $\tau_k(\lambda)$ for the k^{th} color channel and the spectral responsivity $s(\lambda)$ of the camera (Shafer, 1982).

$$I_k(p) = \int_\lambda L(\lambda)\tau_k(\lambda)s(\lambda)\,\mathrm{d}\lambda \tag{1}$$

Equation (1) implies the assumption of a linear camera-chip behavior, i.e. the measured signal at a pixel's location p is proportional to the intensity of the incident light at this position. This assumption generally holds true with little error for CMOS cameras. The spectral transmittance $\tau_k(\lambda)$ and the spectral responsivity of the camera $s(\lambda)$ are often expressed in a combined form as the spectral sensitivity of the camera $S_k(\lambda) = \tau_k(\lambda)s(\lambda)$ for the k^{th} color channel. The term of the camera's spectral sensitivity $S_k(\lambda)$ also includes the wavelength-dependant transmittance of the objective lens $\tau_o(\lambda)$, while the transmittance of the focusing lenses of the light sources can be assumed to be constant in the relevant wavelength-band, as seen in Figure 3. Since spectral integration is a linear transformation, an integration over $L(\lambda)$, which is the combined superposed spectral power distribution of all light sources i via $L(\lambda) = \sum_{i=1}^{n} \int_\lambda L_i(\lambda)$, results in the same camera response as an integration over all light sources $L_i(\lambda)$ and subsequent addition (Klinker et al., 1988). Therefore, equation (1) can be rewritten as

$$I_k(p) = \sum_{i=1}^{n} \int_\lambda L_i(\lambda)S_k(\lambda)\,\mathrm{d}\lambda. \tag{2}$$

Considering that light from the two lateral light sources is reflected on the surface of the droplet, thus creating glare points, the spectral reflectance $r(\lambda, p)$ at pixel position p on the camera sensor is introduced as

$$I_k(p) = \sum_{i=1}^{n} \int_\lambda r(\lambda, p)L_i(\lambda)S_k(\lambda)\,\mathrm{d}\lambda. \tag{3}$$

The spectral reflectance in general is dependant on direction and wavelength of the light incident on the surface and the geometrical shape of the illuminated object. Furthermore the spectral reflectance can be divided into interface (specular) reflection $r_s(\lambda, p)$ and body (diffuse) reflection $r_d(\lambda, p)$, according to the dichromatic reflection model (Shafer, 1984), i.e.

$$r(\lambda, p) = r_s(\lambda, p) + r_d(\lambda, p). \tag{4}$$

For a water droplet, the diffuse reflection $r_d(\lambda, p)$ is neglected due to the smoothness of the surface, so that reflection can be assumed to only be specular reflection $r_s(\lambda, p)$ in the following. Interface

reflection in general is dependent on the index of refraction n following the Fresnel equations (Hecht, 2017). Since the index of refraction is dependant on the wavelength of the incident light $n(\lambda)$, the intensity of both reflected and transmitted light on the interface likewise depend on the wavelength. The neutral interface (NIR) reflection model is a good approximation for a water droplet. It states that the spectral power distribution of the reflected light equals approximately the SPD of the incident light (Lee et al., 1990). This assumption is valid for materials that have an insignificant variation in the index of refraction in the visible spectrum, which holds true for water. With the assumption of dominating specular reflectance and the NIR reflection model the spectral reflectance r becomes independent of the wavelength $r(p) = r_s(p)$ and equation (3) can be rewritten as

$$I_k(p) = \sum_{i=1}^{n} r_{s,i}(p) \int_{\lambda} L_i(\lambda) S_k(\lambda)\, \mathrm{d}\lambda. \tag{5}$$

Since both the spectral power distribution of the the light sources and the spectral sensitivity of the camera are known, an integration over all relevant wavelengths for the camera sensor results in a transfer coefficient

$$t_{k,i} = \int_{\lambda} L_i(\lambda) S_k(\lambda)\, \mathrm{d}\lambda \tag{6}$$

for the transfer of light from each light source L_i to each channel of camera chip I_k.

For the presented measurement setup, consisting of three LEDs with different maximal wavelengths in the red, green and blue spectrum of the visible light (L_r, L_g, L_b) and a camera chip with a red, a green and a blue channel (I_R, I_G, I_B), the resulting transfer function is represented by

$$\begin{pmatrix} I_R \\ I_G \\ I_B \end{pmatrix} = \begin{pmatrix} t_{Rr} & t_{Rg} & t_{Rb} \\ t_{Gr} & t_{Gg} & t_{Gb} \\ t_{Br} & t_{Bg} & t_{Bb} \end{pmatrix} * \begin{pmatrix} r_{s,r} \\ r_{s,g} \\ r_{s,b} \end{pmatrix} = \mathbf{T} * \mathbf{r_s}\,. \tag{7}$$

Finally, the inverse of the transfer matrix $\mathbf{T}$ provides a correction matrix $\mathbf{C} = \mathbf{T^{-1}}$ for a determination of the specular reflection as a result of only a singular light source

$$\mathbf{r_s} = \mathbf{T^{-1}} * \mathbf{I} = \mathbf{C} * \mathbf{I} \tag{8}$$

from the response of the three image channels $\mathbf{I}$. Therefore, the correction function (8) allows for a separation of the images created by each only one of the light sources, resulting in three independent images of the droplet.

4. Results

The images of a water droplet impinging on a substrate with hydrophobic silicon oxide coating recorded for the present work with the above-introduced RGB-Shadowgraphy setup and their

processing are discussed in the following section. The required information for the correction function (8) is calculated from the spectral power distribution of the LED lights and the spectral sensitivity of the camera with the values provided by the manufacturers; see Figure 3.

Figure 4 shows an RGB frame of the droplet shortly after impact and the separated response of the uncorrected channels of the raw image. The comparison of the three separate image channels to the RGB-image demonstrated that the additional information from reflective images of lateral light sources of different wavelength bands can be separated into the channels of an RGB image, which however contain some unwanted crosstalk between the images. Apparently, the background of the green channel is considerably illuminated by the blue light source and the reflective images from the lateral light are apparent on the other channels, but with a lower intensity.

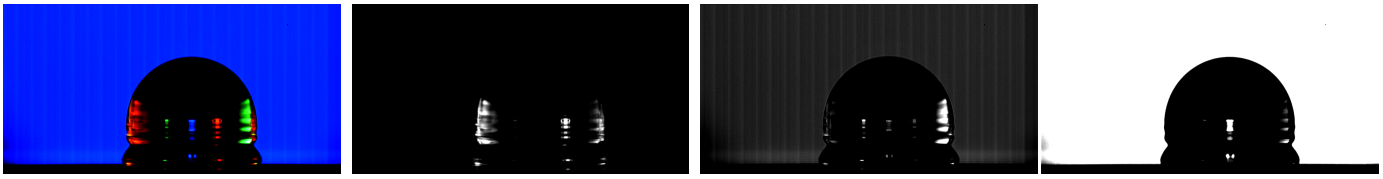

(a) RGB image (b) red (raw) (c) green (raw) (d) blue (raw)

Figure 4. Raw color-imaging of an impinging water droplet on a substrate with SiOx-coating; (a) RGB snap shot; separated (b) red, (c) green and (d) blue raw channels of (a).

(a) RGB image (b) red (corrected) (c) green (corrected) (d) blue (corrected)

Figure 5. Processed color-imaging of an impinging water droplet on a substrate with SiOx-coating; (a) RGB snap shot; separated (b) red, (c) green and (d) blue corrected channels of (a).

As can be seen by the comparison of the results of the spectral correction in Figure 5 to the uncorrected response of the channels in Figure 4, the disturbance of the two other light sources in each channel has been successfully reduced by the correction function (8). This is most saliently emphasized by the removal of the background light in the green channel, as well as the transmitted light around vertical center line resulting from the blue light source. The glare points from the red light source on the right side of the droplet in the green image are reduced as well. In the blue and red channels the glare points from the green light source on the left side of the droplet are likewise removed successfully. The full series of RGB-frames shortly before and after the drop impact is provided in the appendix to further contrast the raw images (Figure 9) to the corrected images (Figure 10).

A quantitative evaluation of the accuracy of the image color correction has been conducted on images from the RGB-imaging for which only one of the light sources was activated. In this setup a

complete color correction is expected to result in zero intensities for all but the considered image channels and only the channel corresponding to the active light source containing an image. The quality of the color correction is measured by the mean image intensity in the omitted image channels, i.e. the remaining disturbance after correction. Figure 6 shows the temporal development of the mean image intensity for all channels in the first 50 images of the drop impact before (dashed lines) and after (solid lines) color correction.

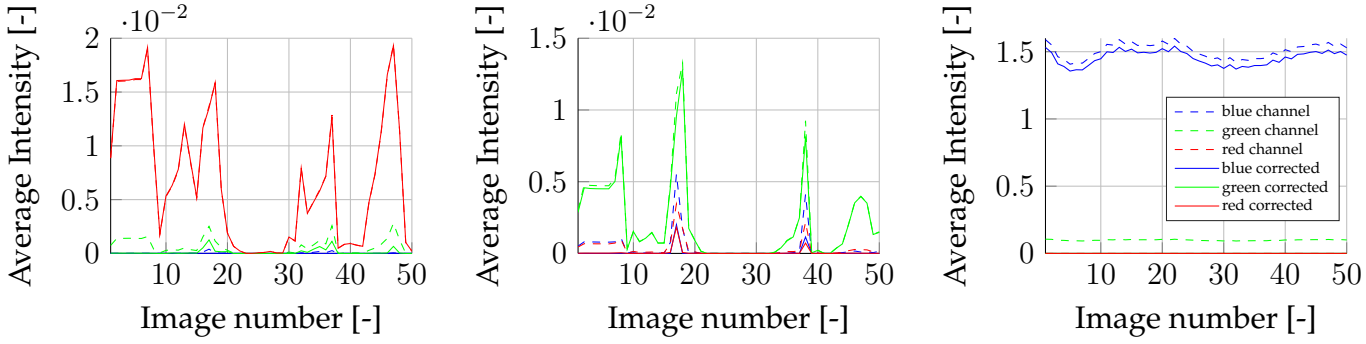

(a) red light (b) green light (c) blue light

Figure 6. Mean image intensities of the unprocessed color channels (dashed lines) in comparison to the corrected color images (solid lines) for the first 50 frames of the drop-impact measurements with a single lateral red (a), green (b) light source or blue backlight (c).

As expected, each light source causes the highest response in the corresponding image channel and additionally a smaller response in each of the two other channels. The intensity of the disturbance in the omitted channels is significantly reduced by the color correction, reaching intensity values of almost zero for most frames, which in turn demonstrates the accuracy of the applied color-correction approach. While the correction of the blue light is nearly perfect, the disturbance in the other channels cannot be fully eliminated for particular frames recorded with only the green or red light source. These frames are characterised by a high overexposure, as can be seen for example in Figure 8, showing the 38^{th} frame of an RGB-Shadowgraphy experiment with only the green lateral light source activated (compare Figure 6 (b)).

5. Discussion

The positive results of the color correction, as seen in Figure 6 suggest that the proposed model and the underlying assumptions are valid. After the color correction, the blue image channel shows only a pure shadowgraphy image without any specular reflection of the lateral light sources. This result demonstrates that the presented method is able to produce standard shadowgraphy images in a high quality with the additional option of further illumination angles of the droplet's interface. While the assumption of a linear response of the chip to the incident light holds true for intensities within the dynamic range, it neglects clipping in the regions of glare points and other highlights. Since one or potentially multiple color channels can be clipped, changes in hue occur (Novak et al., 1990) and a proper calculation of the color correction is inhibited, since the loss of information for

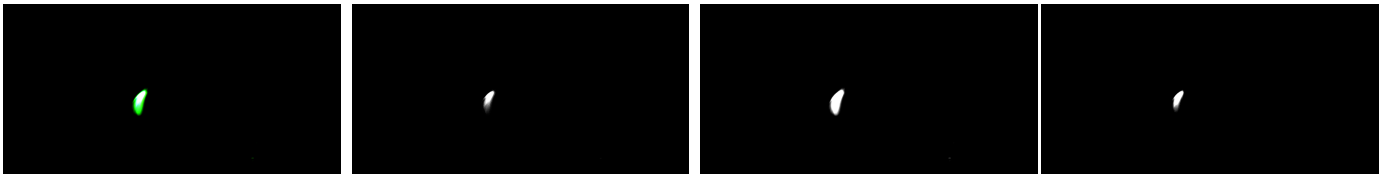

(a) RGB image (b) red (raw) (c) green (raw) (d) blue (raw)

Figure 7. Raw color-imaging with overexposure (frame 38), produced with only the green lateral light source activated; (a) RGB snap shot; separated (b) red, (c) green and (d) blue raw channels of (a).

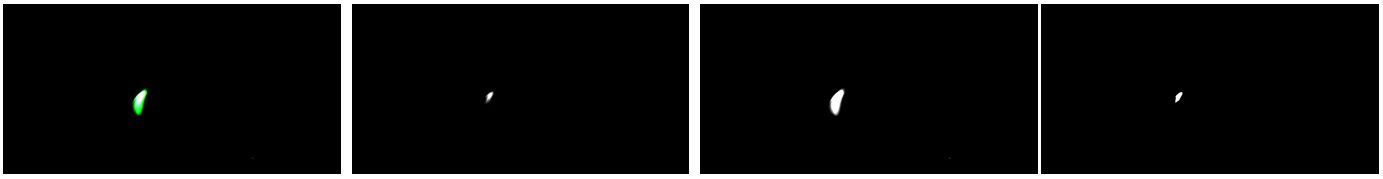

(a) RGB image (b) red (corrected) (c) green (corrected) (d) blue (corrected)

Figure 8. Processed color-imaging with overexposure (frame 38), produced with only the green lateral light source activated; (a) RGB snap shot; separated (b) red, (c) green and (d) blue corrected channels of (a).

intensities above the dynamic range skews the correction function. In the current setup, only a few frames are affected by color clipping, as indicated in Figure 6, and for these frames the correction function does nevertheless improve the distinction of the reflective images. The problem can be mitigated by reducing the intensity of the illumination from the lateral light sources at the cost of a further reduction in the intensity of less pronounced glare points, especially on frames with larger areas of reflection. Therefore, the light source intensity needs to be fine tuned for conserving a maximum of information in dim and bright images.

As can be seen in Figure 10, the illumination of the frames from the lateral light sources varies, depending on the angle of the gas-liquid interface. Mainly vertical interfaces lead to pronounced glare points on the droplet, while horizontal interfaces do no not produce a reflective image. Depending on the droplet dynamics, therefore, some frames contain less information than others, which hinders a reconstruction of the droplet interface. Initial tests revealed that increasing the angle of incidence for the lateral light results in an overall more homogeneous intensity in the glare points over a larger amount of frames. For axisymmetric droplets different incident angles between the two lateral light sources could be exploited to produce a higher number of unique illumination orientations on the droplet, which could e.g. be used in order to detect sites of air entrainment.

It should be noted that the proposed model neglects chromatic aberration and dispersion. Due to the dependence of the refractive index on the wavelength of the incident light the (polychromatic) transmitted light would be deflected at a slightly different angle. Since the transmitted light produces additional glare points on the interface while exiting the droplet and on the interfaces of trapped air bubbles within the droplet, these secondary glare points will be affected by dispersion. As seen in Figure 10 even tertiary and at least quaternary glare points can be observed, each with

an increasing magnitude of dispersion. However the influence of dispersion can be assumed to be negligibly small due to a small change in the index of refraction for the narrow-banded spectrum of the lateral LED light sources. The maximum angular dispersion, i.e. the deviation in the angles of the refracted light, can be estimated to be lower than $0.25°$ for the given spectra using Snell's law (Hecht, 2017) in the first order glare points. Chromatic aberration causes differences in defocus and magnification between the color channels of the image. Therefore, in the presented experiments a Schneider-Kreuznach Apo-Componon 4.0/60 enlarging lens with apochromatic correction has been used to mitigate chromatic aberration. However, further investigation on the effect of chromatic aberration on the quality of the color correction is required.

6. Conclusions and Outlook

In this work it was shown how an extension of the shadowgraphy measurement method by lateral light sources with distinct spectra can be used to gather additional information about the three-dimensional shape of a gas-liquid interface on the example of a liquid droplet impacting on a solid surface. From the spectral power distribution of the light sources and the spectral sensitivity of the camera, a color correction function can be determined by spectral integration, which allows for a clear separation of the two reflection images from the lateral light sources and the shadowgraphy image from the backlight. Therefore, by the means of the proposed color correction function narrow-banded polychromatic light from LEDs can be used to gather three distinct representations of the gas-liquid interface of an impinging droplet.

The presented method of capturing the reflection images from the lateral light sources in each one channel and the shadowgraphy image in the third channel of an RGB-image allows for the use of a simple single-camera setup. This facilitates an easier calibration and reduces the complexity of a volumetric reconstruction from the images in comparison to a multi-camera setup, since no spatial or temporal matching of the produced images is necessary, which would require an exact measurement of the relative positions between the light sources and the camera in respect to the droplet. Note however, that three representations captured with the single-camera RGB-shadowgraphy setup certainly contain less information of the droplet interface than three individual pictures from cameras at different angles.

It was shown that the measurement setup is still able to produce a clear shadowgraphy image that is not impaired by the additional light sources. The two additional channels can be consequently considered as a pure extension to a canonical setup. The additional perspectives from the glare points on the gas-liquid interface by the lateral light sources lay the ground for a volumetric reconstruction of the phase boundary. Since the geometrical properties of the experimental rig – in particular the relative positions of the camera and the light sources in respect to the droplet – are known, features of the droplet surface can be reconstructed by the images of the glare points using the theory of geometrical optics (Healey & Binford, 1988). Lately, vast progress is made in the de-

velopment of deep learning approaches for the volumetric reconstruction from single RGB-images (see Saito et al., 2020; Lin et al., 2018, for instance), in which neural networks learn to infer three-dimensional shapes from image features. Such approaches could be utilized for the volumetric reconstruction of the gas-liquid interface of a droplet during impact. However, grayscale shadowgraphy images do provide only a relatively low amount of features. As such, any additional information encoded in the images by glare points is assumed to facilitate the reconstruction effort with such neural networks.

A strong and continuous measurement signal over the complete range of droplet shapes during impact is required for the reconstruction of the whole droplet dynamics. Therefore, an investigation on the optimal inclination and azimuthal angles of the lateral light sources is necessary. In order to investigate the capability of the proposed method for capturing the three-dimensional droplet impact dynamics during an asymmetric drop impingement further experiments – including the impingement of droplets on structured surfaces – have to be conducted. While the measurement setup was presented along the example of an impinging droplet, it can be expanded to other applications involving gas-liquid interfaces like the two-phase flow in fuel cells, for instance.

References

Ashgriz, N. (2011). *Handbook of atomization and sprays: Theory and applications*. Springer, Heidelberg.

Cox, R. (1986). The dynamics of the spreading of liquids on a solid surface. part 1. viscous flow. *J. Fluid Mechanics*, *168*, 169–194.

Fink, V., Cai, X., Stroh, A., Bernard, R., Kriegseis, J., Frohnapfel, B., … Wörner, M. (2018). Drop bouncing by micro-grooves. *International Journal of Heat and Fluid Flow*, *70*, 271–278.

Healey, G., & Binford, T. O. (1988). Local shape from specularity. *Computer Vision, Graphics, and Image Processing*, *42*(1), 62-86.

Hecht, E. (2017). *Optics*. Pearson, Harlow.

Josserand, C., & Thoroddsen, S. T. (2016). Drop Impact on a Solid Surface. *Annual Review of Fluid Mechanics*, *48*, 365 - 391.

Kistler, S. (1993). Hydrodynamics of wetting. In J. Berg (Ed.), *Wettability* (pp. 311–430). Marcel Dekker, New York.

Klinker, G., Shafer, S. A., & Kanade, T. (1988). The measurement of highlights in color images. *International Journal of Computer Vision*, *2*, 7–32.

Lee, H.-C., Breneman, E., & Schulte, C. (1990). Modeling light reflection for computer color vision. *IEEE Transactions on Pattern Analysis and Machine Intelligence*, *12*(4), 402-409.

Lin, C.-H., Kong, C., & Lucey, S. (2018). Learning efficient point cloud generation for dense 3d object reconstruction. In *Aaai conference on artificial intelligence (AAAI).*

Nitsche, W., & Brunn, A. (2006). *Strömungsmesstechnik*. Springer, Heidelberg.

Novak, C. L., Shafer, S. A., & Willson, R. G. (1990). Obtaining accurate color images for machine-vision research. In M. H. Brill (Ed.), *Perceiving, measuring, and using color* (Vol. 1250, pp. 54 – 68). SPIE.

Rioboo, R., Marengo, M., & Tropea, C. (2002). Time evolution of liquid drop impact onto solid, dry surfaces. *Experiments in Fluids*, *33*, 112-124.

Rioboo, R., Tropea, C., & Marengo, M. (2001). Outcomes from a drop impact on solid surfaces. *Atomization and Sprays*, *11*(2), 155-166.

Saito, S., Simon, T., Saragih, J., & Joo, H. (2020). Pifuhd: Multi-level pixel-aligned implicit function for high-resolution 3d human digitization. In *Proceedings of the ieee conference on computer vision and pattern recognition.*

Shafer, S. A. (1982). Describing light mixtures through linear algebra. *Journal of the Optical Society of America*, *72*(2), 299–300.

Shafer, S. A. (1984). *Optical phenomena in computer vision* (Technical Report TR135). Carnegie-Mellon University, Computer Science Department, Pittsburgh, Pa.

van de Hulst, H. C., & Wang, R. T. (1991). Glare points. *Applied Optics*, *30*(33), 4755–4763.

Wakeham, W. A., Assael, M. J., Marmur, A., Coninck, J. D., Blake, T. D., Theron, S. A., & Zussman, E. (2007). Material Properties: Measurement and Data; Contact Angle. In C. Tropea, A. L. Yarin, & J. F. Foss (Eds.), *Springer handbook of experimental fluid mechanics* (pp. 106–118). Springer, Heidelberg.

Wörner, M., Samkhaniani, N., Cai, X., Wu, Y., Majumdar, A., Marschall, H., … Deutschmann, O. (2021). Spreading and rebound dynamics of sub-millimetre urea-water-solution droplets impinging on substrates of varying wettability. *Applied Mathematical Modelling*, *95*, 53–73.

Yarin, A. (2005). Drop impact dynamics: Splashing, spreading, receding, bouncing…. *Annual Review of Fluid Mechanics*, *38*, 159-192.

Appendix

Comparison of the full series of RGB-frames shortly before and after the drop impact between the raw images (Figure 9) and the corrected images (Figure 10).

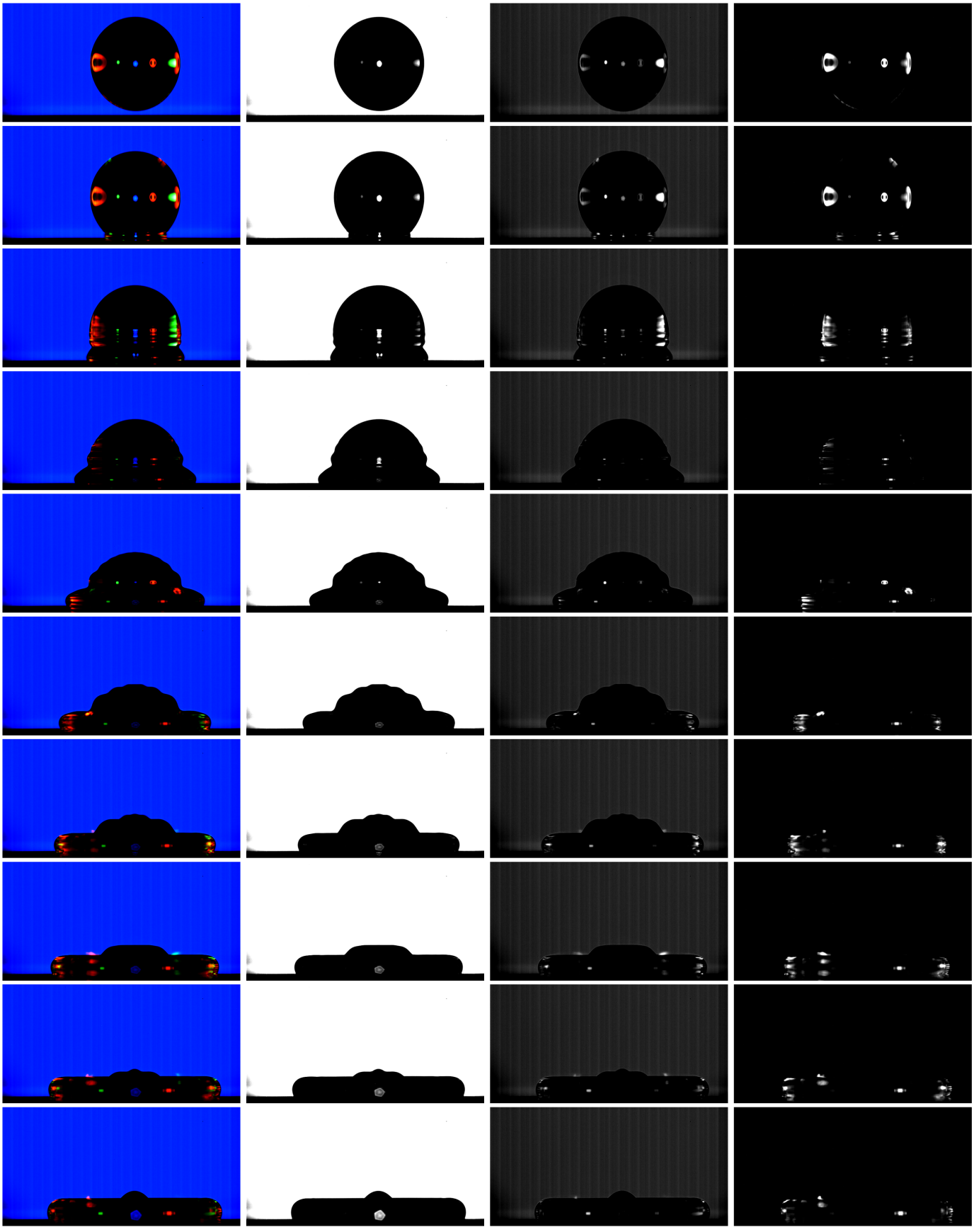

Figure 9. Time series of an impinging water droplet on a substrate with SiOx-coating; (a) RGB snap shots, captured with a *Photron Fastcam Mini WX100* at 3.000 fps; separated (b) red, (c) green and (d) blue raw channels of (a); Note that the third row is a repeated from Figure 4.

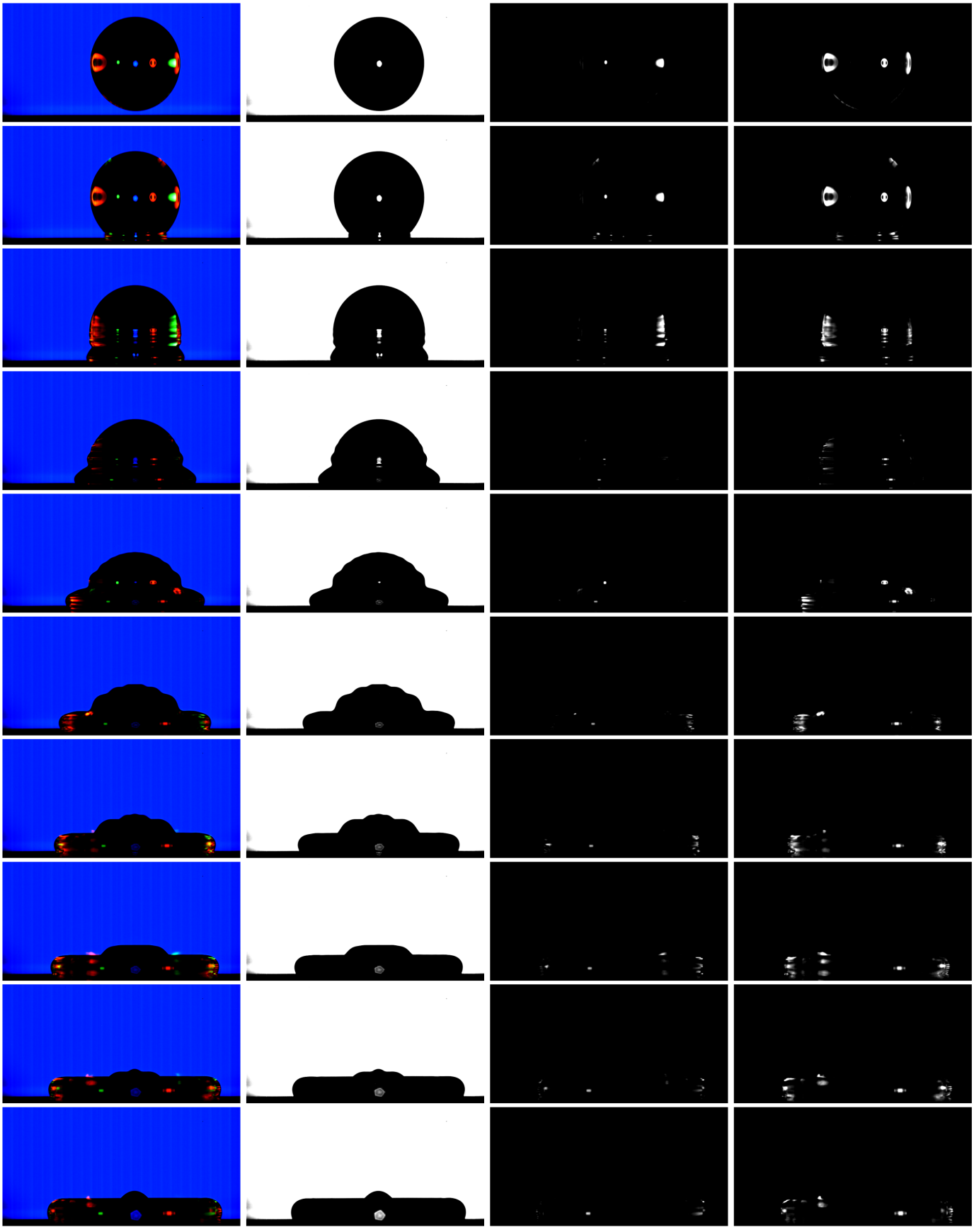

Figure 10. Time series of an impinging water droplet on a substrate with SiOx-coating; (a) RGB snap shots, captured with a *Photron Fastcam Mini WX100* at 3.000 fps; separated (b) red, (c) green and (d) blue raw channels of (a); Note that the third row is a repeated from Figure 5.